Radio-continuum study of Large Magellanic Cloud supernova remnant J0509−6731

L. M. Bozzetto,[1]★ M. D. Filipović,[1] D. Urošević,[2,3] R. Kothes[4] and E. J. Crawford[1]

[1]*School of Computing and Mathematics, University of Western Sydney Locked Bag 1797, Penrith South DC, NSW 1797, Australia*

[2]*Department of Astronomy, Faculty of Mathematics, University of Belgrade, Studentski trg 16, 11000 Belgrade, Serbia*

[3]*Isaac Newton Institute of Chile, Yugoslavia Branch*

[4]*Dominion Radio Astrophysical Observatory, National Research Council Canada, Herzberg Institute of Astrophysics, PO Box 248, Penticton, BBC V2A 6J9, Canada*

ABSTRACT

We present a detailed study of Australia Telescope Compact Array observations ($\lambda = 20$, 13, 6 and 3 cm) of supernova remnant (SNR) J0509−6731 in the Large Magellanic Cloud. The remnant has a ring morphology with brightened regions towards the south-western limb. We also find a second brightened inner ring which is only seen in the radio continuum. The SNR is almost circular, with a diameter ranging from 7 to 8 pc, and a steep radio spectral index between 36 and 3 cm of $\alpha = -0.73 \pm 0.02$, which is characteristic of younger SNRs. We also report detection of radially orientated polarization across the remnant at 6 cm, with a mean fractional polarization level of $P \cong (26 \pm 13)$ per cent. We find the magnetic field ($\sim$168 μG) and $\Sigma - D$ ($\Sigma = 1.1 \times 10^{-19}$ W m^{-2} Hz^{-1} sr^{-1}, $D = 7.35$ pc) to be consistent with other young remnants.

Key words: polarization – ISM: supernova remnants – Magellanic Clouds – radio continuum: ISM.

1 INTRODUCTION

Supernova remnants (SNRs) play a vital role in the Universe, enriching the interstellar medium (ISM) and significantly influences the ISMs evolution, structure and physical properties. The study of SNRs in our own Galaxy is not ideal due to difficulties in estimating accurate distances (which inhibits accurate analysis such as extent and surface brightness) and the high level of absorption in the direction of the Galactic plane. As an alternative, the Large Magellanic Cloud (LMC) at a proximity of 50 kpc (Macri et al. 2006) is a near-ideal galaxy for the study of SNRs due to its high active star-forming regions (such as 30 Dor) and location outside of the Galactic plane at an angle of 35° (van der Marel & Cioni 2001). Its distance from earth allows us to assume that objects located within are at approximately the same distance, aiding in various analysis methodologies.

In the radio continuum, SNRs predominately emit non-thermal continuum emission and generally exhibit a spectrum of $\alpha \sim -0.5$ (defined by $S \propto \nu^\alpha$). Although this can vary as there exists a wide variety of SNRs in different stages of evolution and expanding in different environments (Filipovic et al. 1998).

In this paper, we present new radio-continuum observations of SNR J0509−6731, along with archival radio continuum, X-ray & optical observations. This source was originally classified by Long, Helfand & Grabelsky (1981) as an SNR in their X-ray survey using the *Einstein Observatory*, recording a position of RA (B1950) = $05^h09^m28^s$ and Dec. (B1950) = $-67°34'55''$. Tuohy et al. (1982) estimate an X-ray size of $\sim$25 arcsec, an optical size of 25 arcsec and estimated a shock velocity of >3600 km s^{-1}. No object was found at this position in the 408 MHz image by Clark, Little & Mills (1976). However, reanalysis of the 408 MHz survey data by Tuohy et al. (1982), found weak emission at this point finding a flux density measurement of 95 ± 15 mJy. Tuohy et al. (1982) also observed this object at 5 GHz and measured a flux density of 30 ± 3 mJy. They note that on a surface brightness to diameter ($\Sigma - D$) diagram, SNR J0509−6731 fell below the mean line by a factor of 13, which is comparable to young Galactic SNRs. They comment that this low $\Sigma - D$ might be a result of differences in the electron acceleration process in Balmer dominated remnants. The remnant is described as a Balmer dominated SNR expanding into a region with a relatively low density ($n_H \leq 0.02^{-3}$) of neutral hydrogen and argue for a Type Ia supernova (SN). Mathewson et al. (1983) measure an X-ray size of 27 arcsec and a radio spectrum of $\alpha = -0.46$. Fusco-Femiano & Preite-Martinez (1984) estimate a shock temperature of 3.1 KeV, an age of 900 yr, total swept up mass of 26 M$_\odot$ and a shock velocity of 1600 km s^{-1}, which is well below that proposed by Tuohy et al. (1982) of >3600. Mills et al. (1984) record a 843 MHz flux density of 82 mJy, updating the spectral index to −0.48 and also record a surface brightness of >6.4 × 10^{20} W m^{-2} Hz^{-1} sr^{-1}. van den Bergh (1988) also argues for a younger remnant, commenting that the small diameter indicates an age of ≤1000 yr. Chu & Kennicutt (1988) give this SNR OB association 400 pc to LH38 and class this remnant as Population II. Smith et al. (1991) record

★ E-mail: luke.bozzetto@gmail.com

Table 1. Summary of ATCA observations reduced and used in this study.

Date	Scan time (min)	Right Ascension	Declination	Array	Frequencies (MHz)	BWidth (MHz)	Chan	Project
2011-Nov-16	49.7	$5^h9^m31^s00$	$-67°31'16''20$	EW367	5500, 9000	2048.0	2049	C634[a]
2011-Nov-15	15.0	$5^h9^m31^s00$	$-67°31'16''20$	EW367	5500, 9000	2048.0	2049	C634[a]
2010-Nov-29	98.0	$5^h9^m30^s00$	$-67°30'60''00$	6A	5500, 9000	2048.0	2049	C2367
2010-Nov-28	50.3	$5^h9^m30^s00$	$-67°30'60''00$	6A	5500, 9000	2048.0	2049	C2367
2005-Jun-24	819.7	$5^h9^m51^s48$	$-67°16'22''17$	6B	1384, 1472	128.0	33	C1395
2005-Apr-18	819.8	$5^h9^m51^s48$	$-67°16'22''17$	1.5A	1384, 1472	128.0	33	C1395
1997-Aug-11	643.7	$5^h9^m30^s00$	$-67°30'60''00$	750B	4800, 4928	128.0	33	C479
1994-Sep-23	57.0	$5^h9^m31^s00$	$-67°31'15''00$	1.5D	1380, 2378	128.0	33	C354
1994-Sep-22	482.3	$5^h9^m31^s00$	$-67°31'15''00$	1.5D	1380, 2378	128.0	33	C354
1994-Sep-17	260.7	$5^h9^m31^s00$	$-67°31'15''00$	1.5B	1380, 2378	128.0	33	C354

[a]The observing procedure in this project is described in the text.

Table 2. Integrated flux densities of SNR J0509−6731.

λ (cm)	ν (MHz)	ATCA Project	rms (mJy)	Beam size (arcsec)	S_{Total} (mJy)	ΔS_{Total} (mJy)	Reference
73	408	*MOST*	40	157.3×171.6	95	15	Tuohy et al. (1982)
36	843	*MOST*[a]	0.4	46.4×43.0	111	11	This work
36	843	SUMMS[b]	1.5	48.5×45.0	109	11	This work
20	1373	C354	0.3	21.2×17.3	73	7	This work
20	1377	C373[c]	0.7	40.0×40.0	80	8	This work
20	1381	C1395	0.7	13.0×12.2	79	8	This work
13	2377	C354	0.3	12.3×10.1	51	5	This work
6	4800	Multiple[d]	1.0	35.0×35.0	30	3	This work
6	4800	C479	0.3	28.6×11.8	30	3	This work
6	5000	Parkes	–	300×300	30	3	Tuohy et al. (1982)
6	5500	C634, C2367	0.1	2.6×2.3	31	3	This work
3	8640	Multiple[d]	1.0	22.0×22.0	19	2	This work
3	9000	C634	0.2	22.7×16.0	20	2	This work

[a]From the image described in Mills et al. (1984).
[b]From the image described in Mauch et al. (2008).
[c]From the image described in Hughes et al. (2007).
[d]From the image described in Dickel et al. (2010).

a shock velocity >2000 km s^{-1} and is in agreement with an age of ≤1000 yr. Hughes et al. (1995) note that there is strong emission of elements from silicon to neon and argues for Type Ia SN. Haberl & Pietsch (1999) record an extent of 9.1 arcsec and give this SNR the association [HP99] 542. Warren & Hughes (2004) confirmed that the SN ejecta had an abundance distribution consistent with Type Ia SN explosion models. They also found that the reverse shock is propagating back into the Fe-rich ejecta and suggests that the brightening in the south-west is due to enhanced density in or a deeper penetration of the reverse shock into a portion of the ejecta shell and may be caused by enhanced ambient density or intrinsic asymmetry in the explosion itself. Rest et al. (2005) confirmed the Type Ia classification using light echo spectra and also established it as an SN1991T-type energetic event. Additionally, light echo apparent motion was used to estimate the age of the SNR to be 400 ± 120 yr. Arbutina & Urošević (2005) used a 1 GHz flux density of 70 mJy to estimate a surface brightness–diameter of $(\Sigma - D) = (4.2 \times 10^{-20}$ W m^{-2} Hz^{-1} sr^{-1}, 7 pc). Ghavamian et al. (2007) estimate an age of 295–585 yr, a shock velocity of $V_s \geq 4000$ km s^{-1}, they detect broad Lyβ emission and classify this object as a non-radiative (adiabatic) of Type Ia. Badenes et al. (2008) found an age of ∼400 yr, kinetic energy of 1.4×10^{51} erg and concluded that the X-ray properties of SNR J0509−6731 were consistent with models of an energetic 91T-type SN Ia explosion. Seok et al. (2008) state SNR J0509−6731 is thought to be dominated by thermal dust con-

tinuum with T(dust) 94 ± 3 K and a dust mass of $8.7 \pm 2.5 \times 10^{-5}$ solar masses. Kosenko et al. (2008) also find that the reverse shock has recently reach the iron layers of the ejecta and are in agreement with previous studies regarding the brightening in the south-west resulting from an asymmetric explosion or density enhancement in the ISM. Models in this study were in good agreement with the observations with circumstellar density of 3×10^{-25} g cm^{-3}, age of ∼400 yr and velocity of ∼5000 km s^{-1}. Desai et al. (2010) found no association between this remnant and a young stellar object (YSO), nor the molecular clouds. Schaefer & Pagnotta (2012) found no ex-companion star to a visual magnitude limit of 26.9 within a radius of 1.43 arcsec, which they state would infer a double-degenerate SN system. Di Stefano & Kilic (2012) and Wheeler (2012) discuss the possibility of this SNR still being the result of a single-degenerate explosion.

The observations, data reduction and imaging techniques are described in Section 2. The astrophysical interpretation of newly obtained moderate-resolution total intensity and polarimetric images in combination with archival *Chandra* X-ray and *Hubble Space Telescope* (*HST*) Hα observations are discussed in Section 3.

2 OBSERVATIONS AND DATA REDUCTION

Five Australia Telescope Compact Array (ATCA) projects (C1395, C354, C479, C634 and C2367; at wavelengths of 20, 20/13, 6, 6/3

and 6/3 cm, respectively) were reduced and analysed in this study. A summary of these projects can be seen in Table 1. Project C634 contain our observations of this SNR, which were taken on 2011 November 15 and 16. These observations were taken by the ATCA using the Compact Array Broadband Backend (CABB) receiver with the array configuration EW367, at wavelengths of 3 and 6 cm (ν = 9000 and 5500 MHz). The observations were carried out in the so called 'snap-shot' mode, totalling ∼50 min of integration over a 14 h period. Source PKS B1934-638 was used for primary (flux density) calibration and source PKS B0530-727 was used for secondary (phase) calibration. At 6 cm, the shorter baselines from the EW367 observations were complemented by observations taken from project C2367, which uses a longer baseline array configuration (6A; Table 1), allowing for a higher resolution image. However, we were unable to make use of the 3 cm data from ATCA project C2367 due to strong interference. This lack of data meant we lost the longer baselines and as a result, no high-resolution image is available at this wavelength.

The MIRIAD[1] (Sault, Teuben & Wright 1995) and KARMA[2] (Gooch 1995) software packages were used for reduction and analysis. More information on the observing procedure and other sources observed in this project can be found in Bozzetto et al. (2012a,b,c, 2013) and de Horta et al. (2012).

Images were formed using MIRIAD multifrequency synthesis (Sault & Wieringa 1994) and natural weighting. They were deconvolved with primary beam correction applied. The same procedure was used for both *U* and *Q* Stokes parameter maps.

We measured the flux density of SNR J0509−6731 from 11 separate images between 36 and 3 cm, which are summarized in Table 2. We obtain five of these flux density measurements from available mosaics; at 36 cm from the *Molonglo Synthesis Telescope* (*MOST*) mosaic image (as described in Mills et al. 1984) and from the SUMMS mosaic image (Mauch et al. 2008), 20 cm from the mosaic by Hughes et al. (2007). We also used 6 and 3 cm mosaics published by Dickel et al. (2010). The remaining six measurements were taken from the data reduced and analysed in this study using the projects listed in Table 1. Errors in flux density measurements predominately arose from uncertainties in defining the 'edge' of the remnant. However, we estimate these errors to be <10 per cent (with the exception of the 73 cm measurement, where the associated error is given by Tuohy et al. 1982). Using the flux density measurements in Table 2 (73–3 cm), we estimate a spectral index of $\alpha = -0.59$. However, it can be seen that the spectrum breaks at 73 cm, where the recorded flux density is at a level well below that which is expected (by ∼50 per cent). Low-frequency absorption can result in this 'break', either through synchrotron self absorption or thermal absorption. A low-frequency turnover assumed to be from free–free absorption was found for seven SNRs in M82 (Wills et al. 1997) at levels comparable to our 408 MHz turnover for SNR J0509−6731. However, M82 has an environment significantly denser than the relatively rarefied environment of SNR J0509−6731, and therefore, the turnover is expected to occur at higher frequencies in this denser environment. The more probable explanation for this break is observational effects or an issue with the measurement. Omitting this outlying value from our calculation results in a steeper spectral index with a value of $\alpha = -0.73 \pm 0.02$.
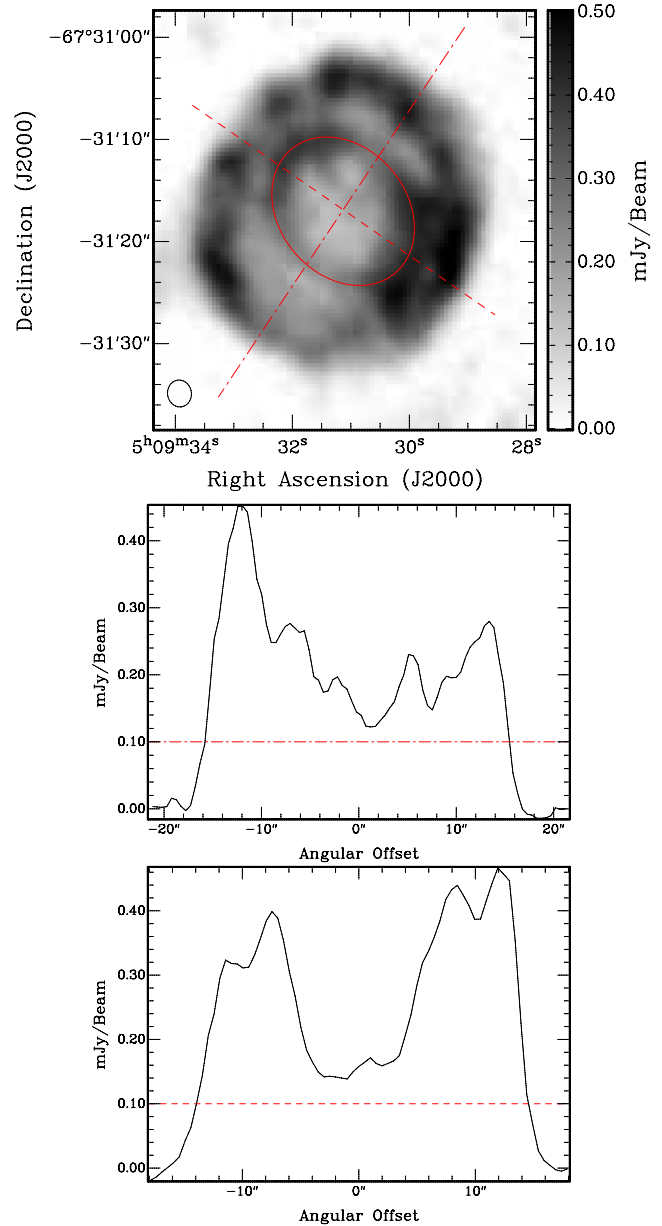
Figure 1. The top image shows the 6 cm intensity image of SNR J0509−6731 overlaid with the approximate major (NW–SE) and minor (NE–SW) axis. The middle and lower images show the one-dimensional cross-section along the overlaid lines in the top image, with a superimposed line at 3σ.

3 RESULTS AND DISCUSSION

SNR J0509−6731 exhibits a ring-like morphology (Fig. 1), centred at RA (J2000) = $05^h09^m31^s.0$, Dec. (J2000) = $-67°31'16''.4$. We estimate the spatial extent of SNR J0509−6731 (Fig. 1) at the 3σ (Table 2; Col. 4) level (0.1 mJy) along the major (NW–SE) and minor (NE–SW) axes (PA = $-34°$). Its size at 6 cm (5500 MHz) is 31 arcsec × 29 arcsec ± 1 arcsec (8 × 7 pc with 0.25 pc uncertainty in each direction). We estimate the ring thickness of SNR J0509−6731 to ∼6 arcsec at 6 cm, about 40 per cent of the SNR's radius.

We find a centrally brightening ring in the interior of this remnant (Fig. 1), something that is not common among SNRs. We estimate
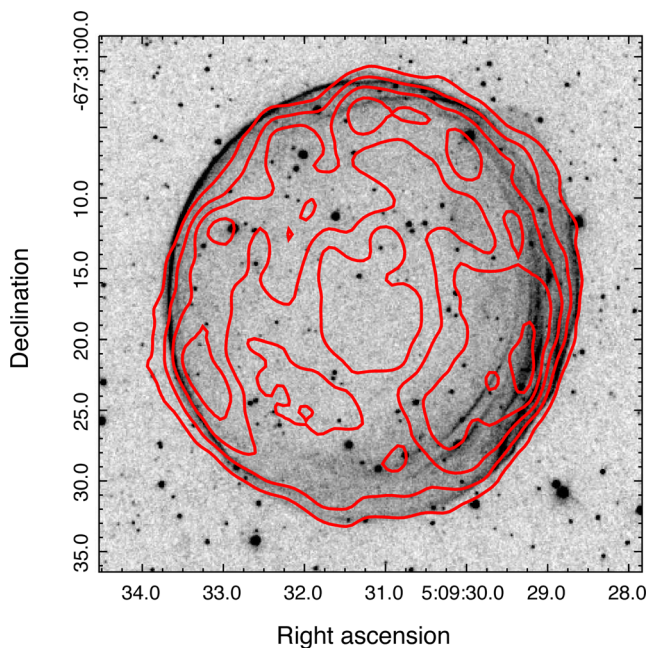
Figure 2. *HST* Hα image of SNR J0509−6731 overlaid with 6 cm ATCA contours. The contours are 3, 6, 9, 12 and 15σ (where σ = 33 μJy).

the size of this ring at 6 cm to be 16 arcsec × 12 arcsec ± 1 arcsec (4 × 3 pc with 0.25 pc uncertainty in each direction) at PA = 50°.

There is evident correlation between our 6 cm (5500 MHz) radio-continuum emission and the optical Hα emission (*HST*; PropID 11015) for this remnant (Fig. 2). This is particularly evident towards the south-western limb of the SNR (where radio emission is the strongest), where we can see the radio 3σ contour closely following the edge of the optical Hα emission. The astrometry involved in aligning all images in this paper is within 1 arcsec.

We also find similarities between our 6 cm (5500 MHz) radio-continuum emission and 0.3–7.0 keV X-ray emission (*Chandra*; observation ID [ObsID] 776[3]) as seen in Fig. 3.

The optical Hα emission shows highly compressed filaments, denoting at high angular resolution the location of the forward shock moving into the ISM, outlying the ellipsoidal shell region interior to which the smooth, low compressed radio and X-ray emission comes.

The non-thermal nature of this remnant in the radio continuum is confirmed in the spectral energy distribution, shown in Fig. 4, where $\alpha_2 = -0.73 \pm 0.02$. This value is steeper in comparison with typical values of $\alpha = -0.5$ for LMC SNRs (Filipović et al. 1998) and is more consistent with young SNRs, shown in Table 3. This is in agreement with current estimation of the remnants age, which places it at ∼400 yr (Rest et al. 2005; Ghavamian et al. 2007; Badenes et al. 2008; Kosenko et al. 2008).

A spectral index map was created between 13 and 6 cm (Fig. 5) to show the spatial spectral variations in the remnant. This was achieved by convolving and re-gridding the 6 cm image with the tasks `regrid` and `convol`, to match the size and resolution of the 13 cm image, which had the poorest resolution and thus allowing no oversampling to occur. A spectral index map was then created using these maps from both observed frequencies. This was done
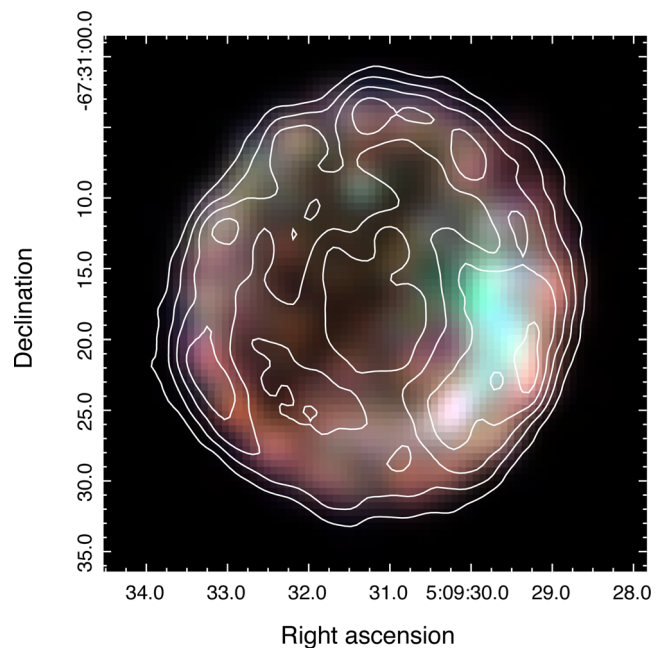
Figure 3. *Chandra* X-ray colour composite image of SNR J0509−6731 at energy levels 0.3–0.6 keV (red) 0.6–0.95 keV (green) and 0.95–7.0 keV (blue). The image has been smoothed using a Gaussian filter (σ = 2 pixels). ATCA radio contours (at 6 cm) have been overlaid at levels of 3, 6, 9, 12 & 15σ (where σ = 33 μJy).
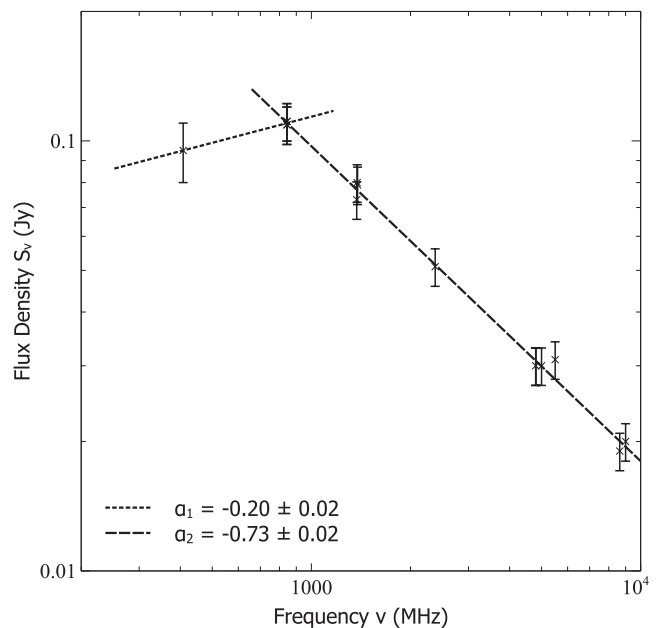

Figure 4. Radio-continuum spectrum of SNR J0509−6731. The markers represent error margins of 10 per cent.

using the MIRIAD task `maths`, which calculated the spectral index[4] (α) of each pixel above a level of 3σ. Pixels below this level were blanked in the spectral index map. We note to two distinctive and opposite regions of somewhat steeper spectra (∼α = −0.7) marked in yellow around northern and southern regions of the SNR.

Table 3. Comparison of SNR J0509−6731 to similar remnants.

Name	Age (yr)	α^*	P (%)	P_λ (cm)	Reference
0509−67.5	~400	−0.73	26 ± 13	6	This work
Cassiopeia A	–	−0.77	8–10	6	Anderson, Keohane & Rudnick (1995)
Tycho	~441	−0.65	20-30[a]	6	Dickel, van Breugel & Strom (1991)
Kepler	~409	−0.64	6	6	DeLaney et al. (2002)
SN 1006	~1000	−0.6	17[d]	20	Reynoso, Hughes & Moffett (2013)
N132D	~2500[b]	−0.70	4	6	Dickel & Milne (1995)
0519−6902	~600[c]	−0.53	2	6	Bozzetto et al. (2012b)

[*]Galactic spectral indices came from the catalogue by Green (2009).
[a]Based on the mean polarization found for the brightened limbs.
[b]Vogt & Dopita (2011).
[c]Borkowski et al. (2006).
[d]Higher polarization (near the theoretical limit of ~70 per cent) was found in regions of weaker radio emission.
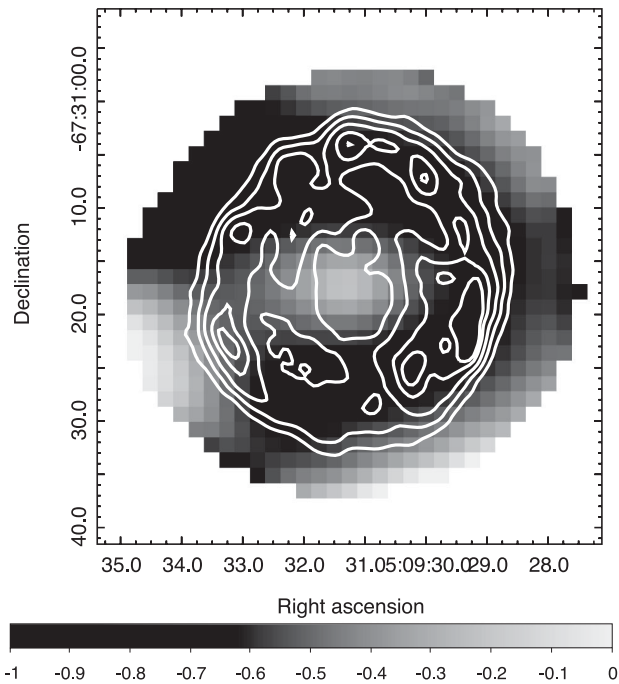

Figure 5. Radio-continuum spectrum map of SNR J0509−6731 between 13 and 6 cm. The sidebar quantifies the spectral index scale. ATCA radio contours (at 6 cm) have been overlaid at 3, 6, 9, 12 and 15σ (where σ = 33 μJy).

A fractional polarization image was created at 6 cm using Q and U parameters (Fig. 6). A signal-to-noise cut-off of 2σ was used for the Q and U images, while a level of 6σ was used for the intensity image. Values that fall below these cut-off levels are blanked in the output image. The length of the vectors has been reduced by 50 per cent and placed every 1.5 pixels for display purposes. The mean fractional polarization was calculated using flux density and polarization:

$$P = \frac{\sqrt{S_Q^2 + S_U^2}}{S_I},$$

where S_Q, S_U and S_I are integrated intensities for the Q, U and I Stokes parameters. We estimate a mean fractional polarization value of $P = 26 \pm 13$ per cent at 6 cm. The magnetic field of the remnant
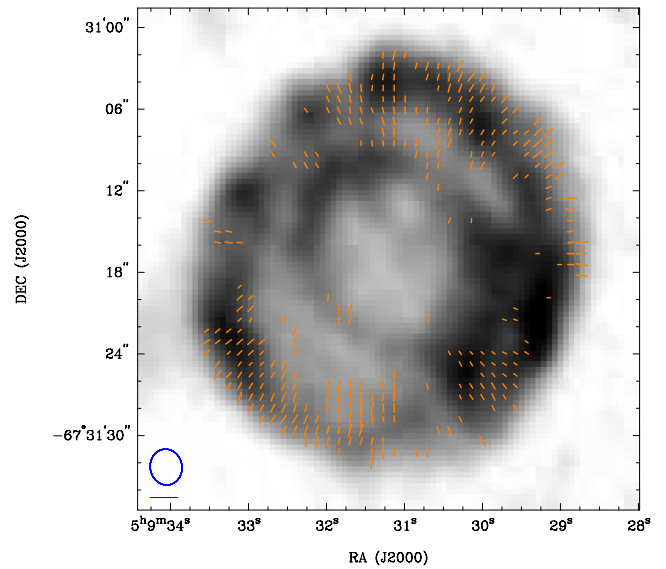

Figure 6. *B*-field polarization vectors overlaid on 6 cm ATCA image of SNR J0509−6731. The blue ellipse in the lower-left corner represents the synthesized beamwidth of 2.6 arcsec × 2.3 arcsec and the blue line below the ellipse represents a polarization vector of 100 per cent.

at 6 cm appears to be radially oriented, which is to be expected from Rayleigh–Taylor instabilities in the decelerating remnant (Gull 1975; Chevalier 1976). This is consistent with similarly young SNRs in our own Galaxy, as well as in the LMC (for e.g. those listed in Table 3).

Without reliable polarization measurements at a second frequency, we cannot determine the Faraday rotation and thus cannot deduce the magnetic field strength. However, we make use of the equipartition formula as given by Arbutina et al. (2012) to estimate the magnetic field strength of this SNR. This formula is based on the Bell (1978) diffuse shock acceleration theory. This derivation is purely analytical, accommodated especially for the estimation of magnetic field strength in SNRs. The average equipartition field over the whole shell of SNR J0509−6731 is ~168 μG with an estimated minimum energy of $E_{min} = 1.2 \times 10^{49}$ erg (see Arbutina et al. 2012; and corresponding 'calculator[5]'). This value is typical of young SNRs with a strongly amplified magnetic field.

[5] The calculator is available at http://poincare.matf.bg.ac.rs/~arbo/eqp/.

The position of SNR J0509−6731 at the surface brightness to diameter ($\Sigma-D$) diagram ($\Sigma = 1.1 \times 10^{-19}$ W m^{-2} Hz^{-1} sr^{-1}, $D = 7.35$ pc) by Berezhko & Völk (2004), suggests that this remnant is in the transition phase between late free expansion and early Sedov phase, with an explosion energy of $\sim 0.25 \times 10^{51}$, which evolves in an environment with a density of ~ 0.3 cm^{-3}. This estimate of minimum explosion energy is lower than that found by Badenes et al. (2008) who found a value of 1.40×10^{51}, a result of using different models. Our estimate of surface brightness is comparable to values found for galactic remnants in rarified environments, such as Tycho's SNR ($\Sigma = 1.32 \times 10^{-19}$ W m^{-2} Hz^{-1} sr^{-1}, $D = 9.3$ pc) and *Kepler*'s SNR ($\Sigma = 3.18 \times 10^{-19}$ W m^{-2} Hz^{-1} sr^{-1}, $D = 5.2$ pc; Pavlović et al. 2013).

4 CONCLUSION

We have used observations taken by the ATCA to carry out a detailed radio-continuum study on SNR J0509−6731. With a size of only $D \cong 8 \times 7$ pc, SNR J0509−6731 is one of the smallest remnants currently known in the LMC. We find a relatively steep spectrum of ($\alpha = -0.73 \pm 0.02$) and relatively strong magnetic field of 168 μG, which is characteristic of a young remnant (e.g. Jiang, Zhang & Fang 2013). Its small size also sets this SNR apart from typical $\Sigma-D$ values of SNRs at $\Sigma = 1.1 \times 10^{-19}$ W m^{-2} Hz^{-1} sr^{-1}, $D = 7.35$ pc, though, still in close proximity to another Balmer-dominated LMC SNR, SNR J0519−6902. This SNR shares the same radially oriented polarization as other young Type Ia remnants, with a mean fractional polarization level of $P = (26 \pm 13)$ per cent.

ACKNOWLEDGEMENTS

REFERENCES

Anderson M. C., Keohane J. W., Rudnick L., 1995, ApJ, 441, 300
Arbutina B., Urošević D., 2005, MNRAS, 360, 76
Arbutina B., Urošević D., Andjelić M. M., Pavlović M. Z., Vukotić B., 2012, ApJ, 746, 79
Badenes C., Hughes J. P., Cassam-Chenaï G., Bravo E., 2008, ApJ, 680, 1149
Bell A. R., 1978, MNRAS, 182, 443
Berezhko E. G., Völk H. J., 2004, A&A, 427, 525
Borkowski K. J. et al., 2006, ApJ, 642, L141
Bozzetto L. M., Filipovic M. D., Crawford E. J., Payne J. L., de Horta A. Y., Stupar M., 2012a, Rev. Mex. Astron. Astrofis., 48, 41
Bozzetto L. M., Filipovic M. D., Urosevic D., Crawford E. J., 2012b, Serb. Astron. J., 185, 25
Bozzetto L. M. et al., 2012c, MNRAS, 420, 2588
Bozzetto L. M. et al., 2013, MNRAS, 432, 2177
Chevalier R. A., 1976, ApJ, 207, 872
Chu Y.-H., Kennicutt R. C., Jr, 1988, AJ, 96, 1874
Clarke J. N., Little A. G., Mills B. Y., 1976, Aust. J. Phys. Astrophys. Suppl., 40, 1
de Horta A. Y. et al., 2012, A&A, 540, A25
DeLaney T., Koralesky B., Rudnick L., Dickel J. R., 2002, ApJ, 580, 914
Desai K. M. et al., 2010, AJ, 140, 584
Di Stefano R., Kilic M., 2012, ApJ, 759, 56
Dickel J. R., Milne D. K., 1995, AJ, 109, 200
Dickel J. R., van Breugel W. J. M., Strom R. G., 1991, AJ, 101, 2151
Dickel J. R., McIntyre V. J., Gruendl R. A., Milne D. K., 2010, AJ, 140, 1567
Filipovic M. D. et al., 1998, A&AS, 127, 119
Fusco-Femiano R., Preite-Martinez A., 1984, ApJ, 281, 593
Ghavamian P., Blair W. P., Sankrit R., Raymond J. C., Hughes J. P., 2007, ApJ, 664, 304
Gooch R., 1995, in Shaw R. A., Payne H. E., Hayes J. J. E., eds, ASP Conf. Ser. Vol. 77, Astronomical Data Analysis Software and Systems IV. Astron. Soc. Pac., San Francisco, p. 144
Green D. A., 2009, Bull. Astron. Soc. India, 37, 45
Gull S. F., 1975, MNRAS, 171, 263
Haberl F., Pietsch W., 1999, A&AS, 139, 277
Hughes J. P. et al., 1995, ApJ, 444, L81
Hughes A., Staveley-Smith L., Kim S., Wolleben M., Filipović M., 2007, MNRAS, 382, 543
Jiang Z. J., Zhang L., Fang J., 2013, MNRAS, 433, 1271
Kosenko D., Vink J., Blinnikov S., Rasmussen A., 2008, A&A, 490, 223
Long K. S., Helfand D. J., Grabelsky D. A., 1981, ApJ, 248, 925
Macri L. M., Stanek K. Z., Bersier D., Greenhill L. J., Reid M. J., 2006, ApJ, 652, 1133
Mathewson D. S., Ford V. L., Dopita M. A., Tuohy I. R., Long K. S., Helfand D. J., 1983, ApJS, 51, 345
Mauch T., Murphy T., Buttery H. J., Curran J., Hunstead R. W., Piestrzynski B., Robertson J. G., Sadler E. M., 2008, VizieR Online Data Catalog, 8081, 0
Mills B. Y., Turtle A. J., Little A. G., Durdin J. M., 1984, Aust. J. Phys., 37, 321
Pavlović M. Z., Urošević D., Vukotić B., Arbutina B., Göker Ü. D., 2013, ApJS, 204, 4
Rest A. et al., 2005, Nature, 438, 1132
Reynoso E. M., Hughes J. P., Moffett D. A., 2013, AJ, 145, 104
Sault R. J., Wieringa M. H., 1994, A&AS, 108, 585
Sault R. J., Teuben P. J., Wright M. C. H., 1995, in Shaw R. A., Payne H. E., Hayes J. J. E., eds, ASP Conf. Ser. Vol. 77, Astronomical Data Analysis Software and Systems IV. Astron. Soc. Pac., San Francisco, p. 433
Schaefer B. E., Pagnotta A., 2012, Nature, 481, 164
Seok J. Y. et al., 2008, PASJ, 60, 453
Smith R. C., Kirshner R. P., Blair W. P., Winkler P. F., 1991, ApJ, 375, 652
Tuohy I. R., Dopita M. A., Mathewson D. S., Long K. S., Helfand D. J., 1982, ApJ, 261, 473
van den Bergh S., 1988, ApJ, 327, 156
van der Marel R. P., Cioni M.-R. L., 2001, AJ, 122, 1807
Vogt F., Dopita M. A., 2011, Ap&SS, 331, 521
Warren J. S., Hughes J. P., 2004, ApJ, 608, 261
Wheeler J. C., 2012, ApJ, 758, 123
Wills K. A., Pedlar A., Muxlow T. W. B., Wilkinson P. N., 1997, MNRAS, 291, 517

This paper has been typeset from a TEX/LATEX file prepared by the author.